

Data-driven optimization of pixelated CdZnTe spectrometers for uranium enrichment assay

Jayson R. Vavrek, Thomas D. MacDonald, Hannah S. Parrilla, Nikhil S. Deshmukh, Mital A. Zalavadia, Benjamin S. McDonald

Abstract—In recent work [Vavrek et al. (2025)], we developed the performance optimization framework `spectre-ml` for gamma spectrometers with variable performance across many readout channels. The framework uses non-negative matrix factorization (NMF) and clustering to learn groups of similarly-performing channels and sweep through various learned channel combinations to optimize the performance tradeoff of including worse-performing channels for better total efficiency. In this work, we integrate the `pyGEM` uranium enrichment assay code with our `spectre-ml` framework, and show that the U-235 enrichment relative uncertainty can be directly used as an optimization target. We find that this optimization reduces relative uncertainties after a 30-minute measurement by an average of 20%, as tested on six different H3D M400 CdZnTe spectrometers, which can significantly improve uranium non-destructive assay measurement times in nuclear safeguards contexts. Additionally, this work demonstrates that the `spectre-ml` optimization framework can accommodate arbitrary end-user spectroscopic analysis code and performance metrics, enabling future optimizations for complex Pu spectra.

I. INTRODUCTION

The H3D M400 gamma spectrometer [1] is being adopted by the International Atomic Energy Agency (IAEA) as its primary in-field uranium enrichment non-destructive assay (NDA) technology [2], [3], [4]. The M400 features four CdZnTe (CZT) crystals each pixelated to an 11×11 grid, and offers medium resolution gamma spectroscopy at room temperature in a compact form factor. In previous work, we showed that the spatial variations in detector performance [5] within the CZT crystal volumes could be exploited to optimize spectroscopic performance metrics [6]. In particular, a balance can be found between identifying and rejecting poorly-performing detector regions (e.g., the poor-resolution anode regions and/or poor-signal-to-background cathode regions as shown in Fig. 1, or pixels with high defect concentrations [7]) and the associated loss of efficiency. Because of the large number of possible voxel combinations ($\sim 10^{7285}$), computing the globally optimum set of voxels to include is infeasible, and approximate, data-driven methods were developed. Several of the example optimizations therein focused on minimizing the

J.R. Vavrek, T.D. MacDonald, and H.S. Parrilla are with the Nuclear Science Division, Lawrence Berkeley National Laboratory, Berkeley, CA, 94720, USA. N.S. Deshmukh, M.A. Zalavadia, and B.S. McDonald are with the National Security Directorate, Pacific Northwest National Laboratory, Richland, WA, 99354, USA.

The work presented in this paper was funded by the National Nuclear Security Administration of the Department of Energy, Office of International Nuclear Safeguards. This work was performed under the auspices of the U.S. Department of Energy by Lawrence Berkeley National Laboratory (LBNL) under Contract DE-AC02-05CH11231.

relative uncertainty in a peak fit amplitude parameter as proofs of concept in lieu of more advanced spectral performance metrics.

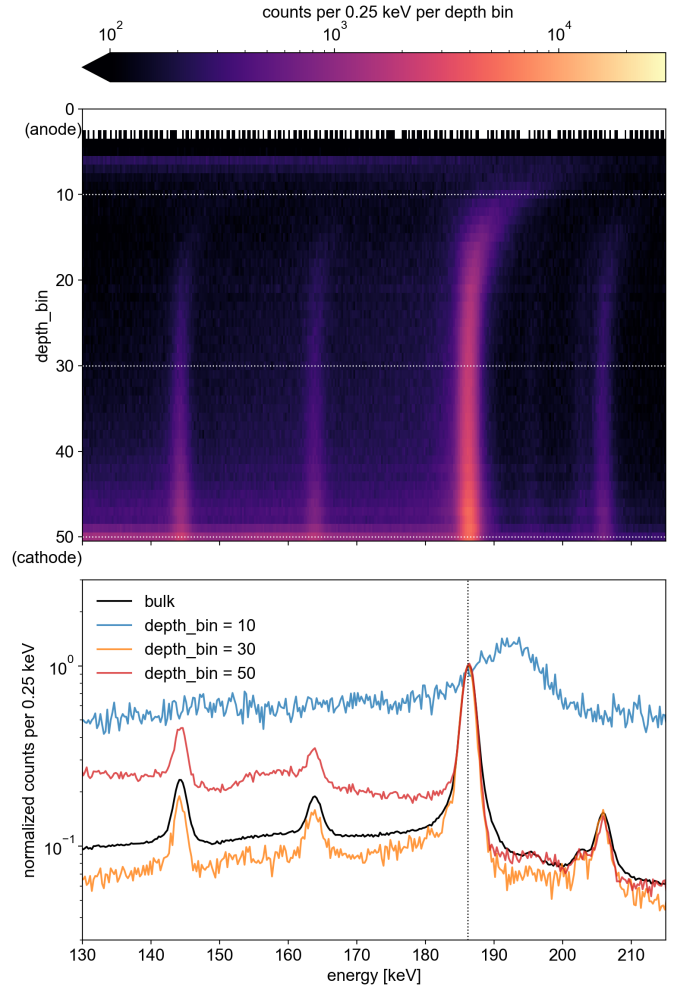


Fig. 1. Uranium gamma spectra as a function of depth in the PNNL M400 detector. Top: heatmap of all depth spectra. The white dotted lines indicate the depth bin selections used in the bottom panel. Bottom: bulk spectrum and spectra at three depth bin selections, each normalized to their intensity at 186 keV (black dotted line) to better show their shapes. Depth bins near the anode degrade in resolution and can exhibit gain drifts, while depth bins near the cathode have increased backgrounds.

In this work, we have integrated our spectroscopic optimization software `spectre-ml` with GEM [8], the actual software used by the IAEA to conduct uranium NDA measurements. We show that the relative uncertainty on the GEM enrichment calculation can directly be used as a `spectre-ml` optimization

target, i.e., that `spectre-ml` can improve the statistical confidence of the IAEA’s in-field enrichment measurements without increasing measurement times, or conversely can achieve the same statistical confidence in shorter measurement times. Similarly, `spectre-ml` improvements could widen the pool of CZT crystals meeting the performance requirements necessary for in-field measurements, potentially driving down manufacturing costs. Such software-based optimization could reduce the need for and/or complement various hardware-based advances such as design stage optimizations [9, §3.2], [10] that do not account for individual crystal differences, digital pulse processing for improved energy resolution [11] [12, §5.2], and the use of the more spatially-homogeneous CdZnTeSe [13] instead of CZT.

This paper is structured as follows: Section II covers the integration of the `spectre-ml` and GEM codes at a high level, discussing recent improvements to the former to better enable arbitrary end-user workflows, and providing an overview of the GEM workflow itself. It also describes the uranium measurements and optimization parameter sweeps used for analysis. Section III gives the results of six GEM-based `spectre-ml` optimizations for six M400 units, showing that the enrichment relative uncertainty can be directly used as an optimization target. Section IV then provides additional interpretation of the results, discusses some limitations, and suggests avenues for further work. Finally, the Appendix gives a pseudocode overview of how an end-user can integrate their own spectrum analyses into the `spectre-ml` optimization framework.

II. METHODS

A. Integration of the `spectre-ml` and `pyGEM` codes

The `spectre-ml` [6], [14] code is a Python package for optimizing the performance of many-channel gamma spectrometers by intelligently rejecting data from poorly-performing detector channels (i.e., spatial regions). It uses non-negative matrix factorization (NMF) [15], [16] and unsupervised clustering algorithms to learn groups of voxels with similar performance, compute performance metrics across various voxel cluster combinations, and then sweep over hyperparameters such as clustering algorithm, number of clusters, number of NMF components, etc., to find the best overall set of voxels to include. Previous versions of `spectre-ml` were restricted to single Doniach [17] or Gaussian peak fit workflows using the `becquerel` library for peak fits. In this work we have generalized the `spectre-ml` software to abstract out the dependence on `becquerel` and enable arbitrary user-defined spectrum analyses, in particular those based on GEM. The `pyGEM` [18] code is a Python interface to the General Enrichment Measurements (GEM) code [8] used by the IAEA for uranium enrichment NDA. It fits measured spectra in the ~ 120 – 270 keV region of interest using a set of known U-235 emission lines, forward scatter, and high-energy downscatter profiles, and has recently been updated to handle the asymmetric peak shapes of CZT. In contrast to our Doniach fit `becquerel` workflow, `pyGEM` uses a triple-Gaussian model for each peak in CZT—one primary peak, one low-energy tail, and one high-energy tail. The user provides `pyGEM`

a spectrum from a sample of known U-235 enrichment, and it will then compute a linear calibration between the fit net count rate in the 185.7 keV peak and the U-235 atom abundance that can be used to compute the enrichment from an unknown sample spectrum. It is also possible to incorporate correction factors for certain changes between the calibration and sample spectra such as changes in the sample matrix (e.g., U metal vs. U_3O_8), Al and steel wall thicknesses, etc. The `pyGEM` enrichment relative uncertainty calculation incorporates both statistical and systematic (i.e., fit error) components, and thus the `spectre-ml` optimization can be viewed as trading off statistical vs. systematic uncertainties as voxel clusters with higher fit error are removed.

To integrate the two codes, some `spectre-ml` updates were required to handle both the `becquerel` and `pyGEM` workflows. As shown in the pseudocode in the Appendix, `spectre-ml` now provides the abstract base classes `SpectrumAnalyzer` and `RankingMetric`. The user must provide concrete subclasses implementing `SpectrumAnalyzer.analyze` and `RankingMetric.calc`, where the latter method takes a spectrum analyzed (e.g., fit) by the former and extracts a single float metric such as the relative uncertainty in a fit parameter (`becquerel`) or in an enrichment (`pyGEM`) calculation. The usual `spectre-ml` analysis then proceeds and the various voxel selections tested are then ranked by these metric values, with the best metric value indicating which voxel selection to use for the given application defined by the input spectra and choice of spectrum analysis and ranking metric. An overview of the pipeline is given in Fig. 2. We note that no `pyGEM` code changes were required, indicating that `spectre-ml` end-users can relatively easily slot in their own analysis routines.

B. Uranium enrichment assay optimization

Multiple U_3O_8 standards measurements were performed with six US National Laboratory M400 detectors (Brookhaven, Idaho, Los Alamos, Oak Ridge, Pacific Northwest, and Sandia National Laboratories) [12] and provided to Lawrence Berkeley National Laboratory for analysis with `spectre-ml`. In this work we use the 30-minute collimated M400 measurements of Standard Reference Material (SRM) 969 [19] samples with label U-235 enrichments of 1.94 wt% and 4.46 wt% (certified values of (1.9420 ± 0.0014) wt% and (4.4623 ± 0.0032) wt%). The latter is used as the known-enrichment sample for the `pyGEM` activity calibration while the former is used as the unknown sample to be assayed.

The relative uncertainty in the U-235 enrichment is a crucial performance metric for U-235 NDA as it is directly used in computing the *operator-inspector difference* (OID) in terms of z -scores or “sigmas”, and used to compare uncertainties against the International Target Values (ITVs) for the GEM-based verification method [20]. A lower relative uncertainty on the measured U-235 enrichment increases the statistical power of the measurement to detect diversions from declared enrichments and thus potential treaty violations. Since the statistical component of the relative uncertainty decreases with

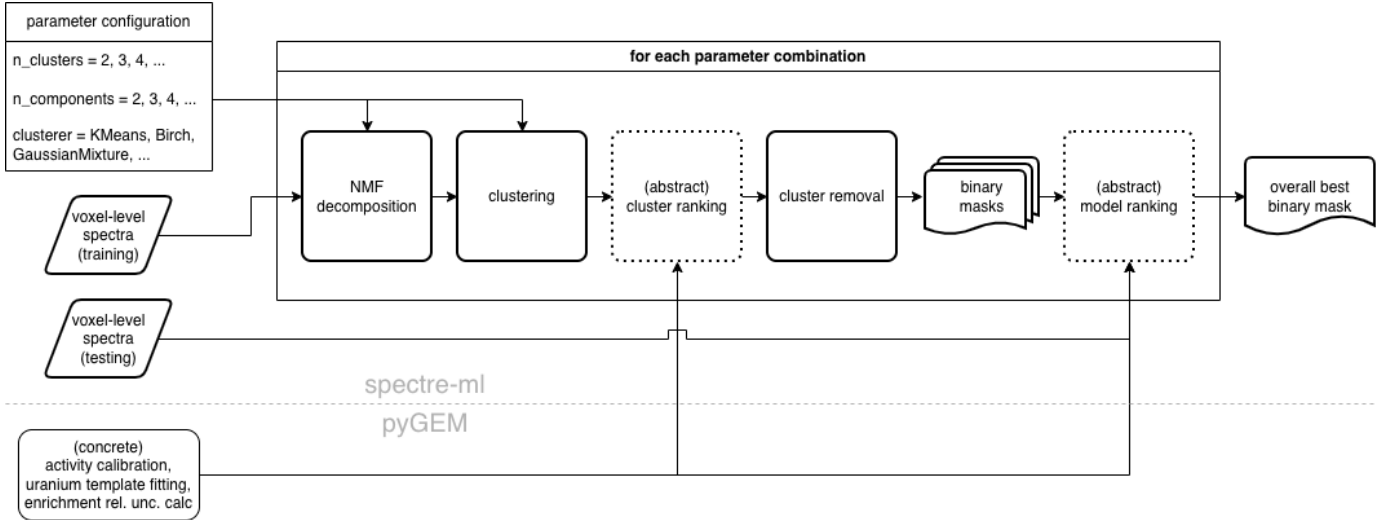


Fig. 2. Overview of the `spectre-ml + pyGEM` pipeline, adapted from Fig. 2 of Ref. [6].

the square root of measurement time, long measurement times may be required for high statistics; longer measurement times are however not always an option for inspectors performing verifications in the field. Optimizing for lower relative uncertainty can therefore improve the time-efficiency of IAEA NDA tasks.

It is also useful to quantify improvements in the `pyGEM` fit quality after voxel clusters are removed. A `pyGEM` analysis typically uses the “`Nqfit`” metric, an “intensity-normalized” version of the standard reduced chi-squared χ^2_ν , given by [21]

$$\text{Nqfit} - 1 = (\chi^2_\nu - 1) \frac{100 \times 10^3}{\text{sum} + 50 \times 10^3}. \quad (1)$$

Here `sum` is the total counts of the U-235 fit component, such that `Nqfit` is essentially a χ^2_ν scaled to an assumed “normal” counting statistics of 50×10^3 counts.

In the optimization examples of Section III, the `spectre-ml` optimization considers four different classes of algorithms for creating voxel clusters (see also Ref. [6]):

- 1) machine learning (ML): standard machine learning clustering algorithms, e.g., Gaussian Mixture, Agglomerative, or k -means clustering, using the NMF spectral decomposition weights as inputs;
- 2) heuristic:
 - a) equal-depth: segments the detector into n_{clus} equally-sized regions in depth;
 - b) edge-and-anode: segments the detector into three regions: a depth region of n_{anode} depth bins, an edge region of the n_{edge} outer pixels of each of the four detector modules (not including the anode depth bins), and the rest of the detector volume;
- 3) greedy: computes the metric directly on spectra within every distinct spatial element (voxel, pixel, depth bin, or crystal), ranks each element by its individual metric, then successively clusters elements together in that order;
- 4) random: assigns n_{clus} random cluster labels at the voxel, pixel, depth bin, or crystal level.

The ML parameter sweeps consist of $n_{\text{clus}} = 2\text{--}6$ clusters (Gaussian Mixture only), $n_{\text{comp}} = 2\text{--}6$ NMF components, and $\alpha_W = 0.0$ (i.e., no NMF regularization). The equal-depth and edge-and-anode algorithms use $n_{\text{clus}} = 2\text{--}6$ and a fixed $(n_{\text{edge}}, n_{\text{anode}}) = (1, 15)$, respectively. The greedy detector algorithm is used, but not the greedy pixel, depth bin, or voxel algorithms due to memory constraints, and a single sample is run for each of the random pixel, depth bin, and voxel clusters with $n_{\text{clus}} = 2\text{--}6$.

III. RESULTS

Fig. 3 shows the results of the `spectre-ml + pyGEM` U-235 enrichment relative uncertainty optimization using the PNNL M400 uranium standards dataset. The enrichment relative uncertainty of 1.06% from the bulk (unoptimized) spectrum is improved to 0.93% (a relative improvement of 12%) when using $n_{\text{comp}} = 3$ and retaining 1 out of 3 Gaussian Mixture clusters. This voxel mask reduces the 185.7 keV net peak area from 8.22×10^5 cps to 4.45×10^5 cps (an efficiency reduction to 54% of the unoptimized detector) and slightly degrades the peak full width at half maximum (FWHM) from 1.18% to 1.20%, but improves the overall fit quality `Nqfit` from 2.70 to 1.93 by reducing fit residuals in both continuum and photopeak regions. The top 5 masks achieve similar final metrics of 0.93%–0.94%. The Gaussian Mixture clusterer generally outperforms the heuristic clustering algorithms, since it can learn and better represent trends in a particular dataset. The edge-and-anode and random pixel and voxel clusterers achieve results worse than the bulk value of 1.06%, due in part to their inability to learn from the data, but also their more limited parameter sweeps.

Similar or better `spectre-ml + pyGEM` improvements in the U-235 enrichment relative uncertainty are observed across all six M400 detectors tested—see Table I. The metric relative improvements range from 12% to 26%, with a mean of 20%. Four out of six detectors are best improved by a GaussianMixture clusterer with 2 out of 3 clusters retained, while the PNNL detector removes one additional cluster and

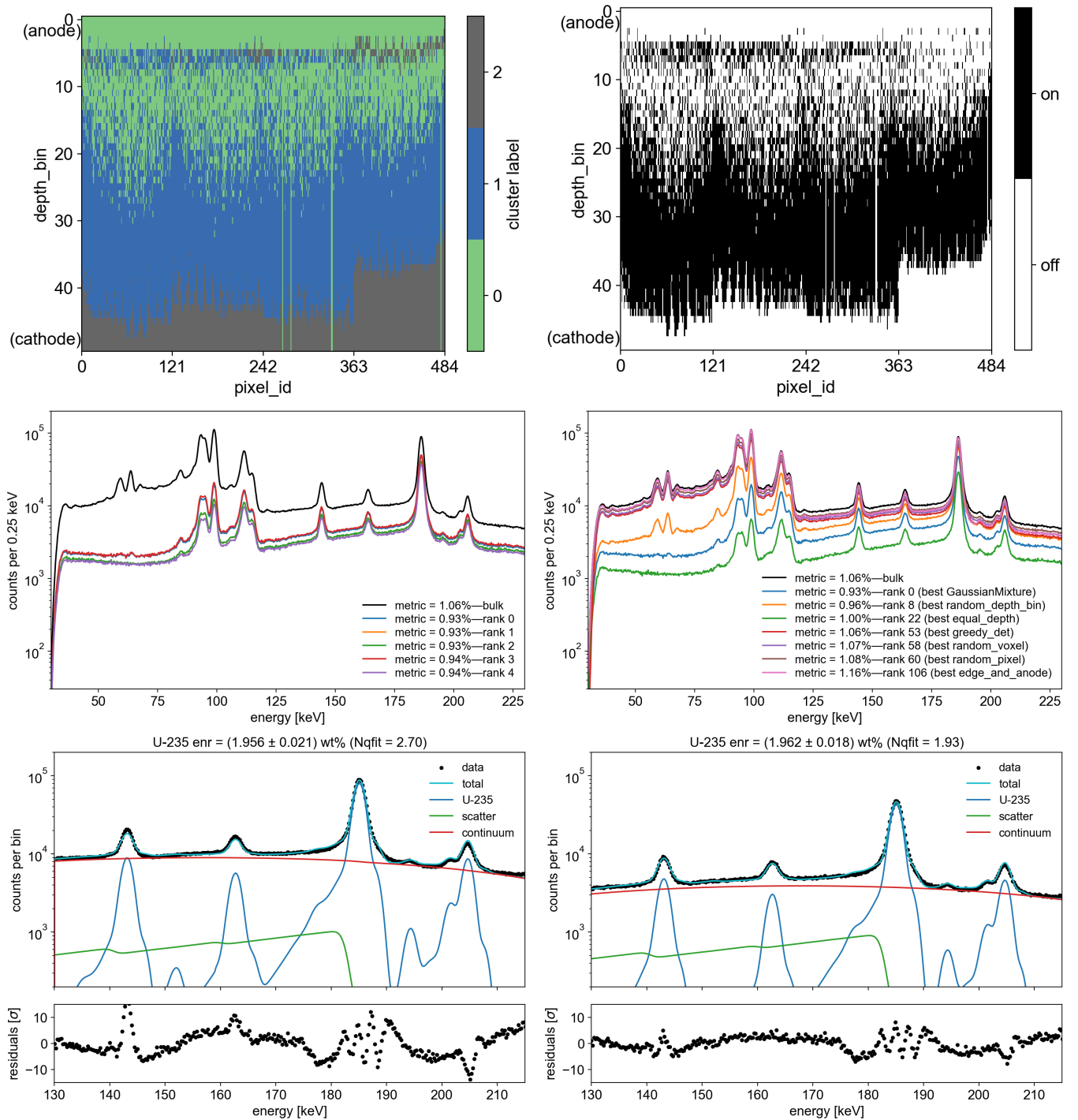


Fig. 3. Uranium enrichment relative uncertainty optimization example with the PNNL M400 detector. Top left: best cluster labels. Top right: best cluster mask. Center left: top 5 spectra ranked by enrichment relative uncertainty. Center right: best spectrum from each class of clustering algorithm. Bottom left: `pyGEM` fit to the bulk spectrum. Bottom right: `pyGEM` fit to the best spectrum.

the BNL detector sees best results from the random depth bin clusterer—see the best cluster masks in Fig. 4. These six masks, though found for different detectors via different model parameters, all remove largely depth-based clusters, mostly near the cathode and/or anode. CZT resolution degradation near the anode is well-known [22], and worse signal-to-background ratios are observed near the cathode in Fig. 1. See also the discussion on the similarity of the six masks in Section IV. The relative efficiencies after voxel cluster removal range from 54% (PNNL) to 70% (BNL), with the remaining four detectors more tightly grouped between 61% and 68%. All optimizations produce very small FWHM degradations, on average changing from 1.15% (bulk) to 1.21% (best), for reasons that are not yet known. Finally, the `pyGEM` fit quality improves in all six optimizations, from an average `Nqfit` of 2.81 to 1.71.

The analyses above were run with the full 30-minute dwell time datasets, where systematic fit uncertainty is expected to dominate over statistical counting uncertainty. To expand this analysis, we also test the performance of these long-dwell-computed masks on shorter sub-samples of the same data. Fig. 5 shows the U-235 enrichment (wt%) and its relative uncertainty (the direct optimization metric) as a function of dwell time t for three of the six detectors. As expected, the relative uncertainty decreases with increasing dwell time, for both the bulk and optimized results. The *initial* optimized relative uncertainty tends to be larger than the initial bulk value, presumably due to worse counting statistics from the lower efficiency, but the rate of decrease in the optimized curves is faster, leading to a *crossover time*, t^* , where the optimized relative uncertainty first falls below the bulk result. As shown in Table II, these crossover times range from 17 s to 117 s, with an average of 49 s, depending on the detector. Similarly, we can quantify the *speedup factor*, f_t , that could be achieved by dwelling with the optimized model only until the relative uncertainty from the bulk dataset at time t is reached. For the full 30-minute datasets, these speedups f_{30} range from $5.2\times$ to $15.4\times$, with an average of $10.3\times$, and are also given in Table II. For a shorter 5-minute dwell time, the speedups f_5 range from $2.3\times$ to $5.2\times$, with an average of $3.8\times$, indicating that the optimized models can achieve the same relative uncertainty as a 5-minute bulk measurement in about a quarter of the time.

In addition to the improvement in the relative uncertainties in Fig. 5—the precisions of the enrichment calculations—it is also important to discuss the effects on the accuracies. The INL, SNL, and LANL detector datasets in Fig. 5 were specifically chosen to highlight three different cases: the bulk detector accuracy is essentially unchanged by the optimization (INL); it is slightly improved by the optimization (SNL); and it is slightly degraded by the optimization (LANL). Similarly, Fig. 6 summarizes the U-235 enrichment assay results for all six detectors. The LANL M400 result appears to be an outlier that pulls the six-detector mean above the sample’s declared enrichment band, but other than the LANL detector, each detector result agrees within error bars. Three of the six detectors have computed U-235 enrichments closer to the declared value without using the `spectre-ml` optimization, and three of

six are closer with it. With or without the `spectre-ml` optimization, the computed enrichments can fall on either side of the declared value—but with the optimization, the uncertainties are improved without any obvious bias.

IV. DISCUSSION

The results of Section III demonstrate that `spectre-ml` can improve uranium enrichment assay uncertainties found via the `pyGEM` code, thereby offering faster measurement times for in-field safeguards inspections. Here we discuss a handful of remaining limitations, and present opportunities for future work.

First, the `spectre-ml` parameter sweeps are much smaller than those used in Ref. [6], using only 2–6 clusters and NMF components, only the Gaussian Mixture clusterer (among the ML options), and no NMF regularization. It is likely that the observed 20% average relative improvement in the U-235 enrichment relative uncertainty metric would improve if the parameter sweeps were expanded. Currently, we are compute-limited by the worse performance of the underlying `scikit-learn` libraries on the Windows machine required for the `pyGEM` code, with even these smaller parameter sweeps taking >1 hr wall time on a 4-core 11th Gen Intel Core i7-1185G7 processor. Performance is also degraded by some difficult-to-avoid array copies in the `pyGEM` pipeline, as well as the need to run both NMF and fitting routines on spectra of $O(1000)$ bins for the entire U-235 region rather than the $O(100)$ bins for a single photopeak. Better parallelization, either in the `scikit-learn` routines or over individual parameter combinations, could greatly improve the speed of the optimization.

We also note that the observed 20% average relative improvement is smaller than the $\sim 3\times$ improvement observed in the U-235 peak analysis of Ref. [6], as expected, due to the much lower systematic fit error arising from the more complex spectrum fit (which includes the 195 keV peak) in `pyGEM`. This re-emphasizes the importance of carefully defining the performance metric to be used to avoid specification gaming.

The similarity of four out of six best voxel removal models in Table I and therefore masks in Fig. 4 suggests that a single common mask could be applied to improve many M400 detectors without having to specifically optimize each detector, even despite inter-detector performance differences. It would be valuable in the future to quantify this level of mask transferability among detectors.

Our analysis here has been limited to using the 4.46%-enriched U-235 standard as a calibration standard for assaying the 1.94%-enriched sample. In the future, it could be interesting to repeat the analysis for the reverse combination, and to include the 20.11%-enriched measurements from the same collection of datasets. Similarly, other safeguards measurement scenarios such as UF_6 cylinders could be considered.

Finally, we note that the ease with which `pyGEM` was integrated with `spectre-ml` bodes extremely well for future integrations of other analysis codes and/or other detector arrays. For instance, FRAM [23] could be integrated to test the ability of `spectre-ml` to improve the challenging analysis of multiple densely-packed photopeaks in Pu spectra.

TABLE I
SUMMARY OF spectre-ml + pyGEM U-235 ENRICHMENT ASSAY OPTIMIZATION RESULTS ACROSS SIX M400 DETECTORS.

detector	BNL	INL	LANL	ORNL	PNNL	SNL	mean
best model (n_{comp} ; n_{clus})	—	6; 2 of 3	5; 2 of 3	2; 2 of 3	4; 1 of 3	4; 2 of 3	—
186 keV rel. eff.	70%	62%	61%	68%	54%	65%	63%
U-235 wt%, bulk	1.974 ± 0.020	1.935 ± 0.020	1.951 ± 0.020	1.938 ± 0.019	1.956 ± 0.021	1.875 ± 0.021	1.938 ± 0.008
U-235 wt%, best	1.959 ± 0.018	1.937 ± 0.015	2.004 ± 0.016	1.950 ± 0.014	1.962 ± 0.018	1.901 ± 0.016	1.952 ± 0.007
metric improvement	13%	24%	21%	24%	12%	26%	20%
186 keV FWHM, bulk	1.12%	1.13%	1.15%	1.20%	1.18%	1.10%	1.15%
186 keV FWHM, best	1.14%	1.21%	1.24%	1.32%	1.20%	1.14%	1.21%
pyGEM fit quality, bulk	2.78	2.78	2.73	2.47	2.70	3.37	2.81
pyGEM fit quality, best	2.05	1.55	1.62	1.37	1.93	1.76	1.71

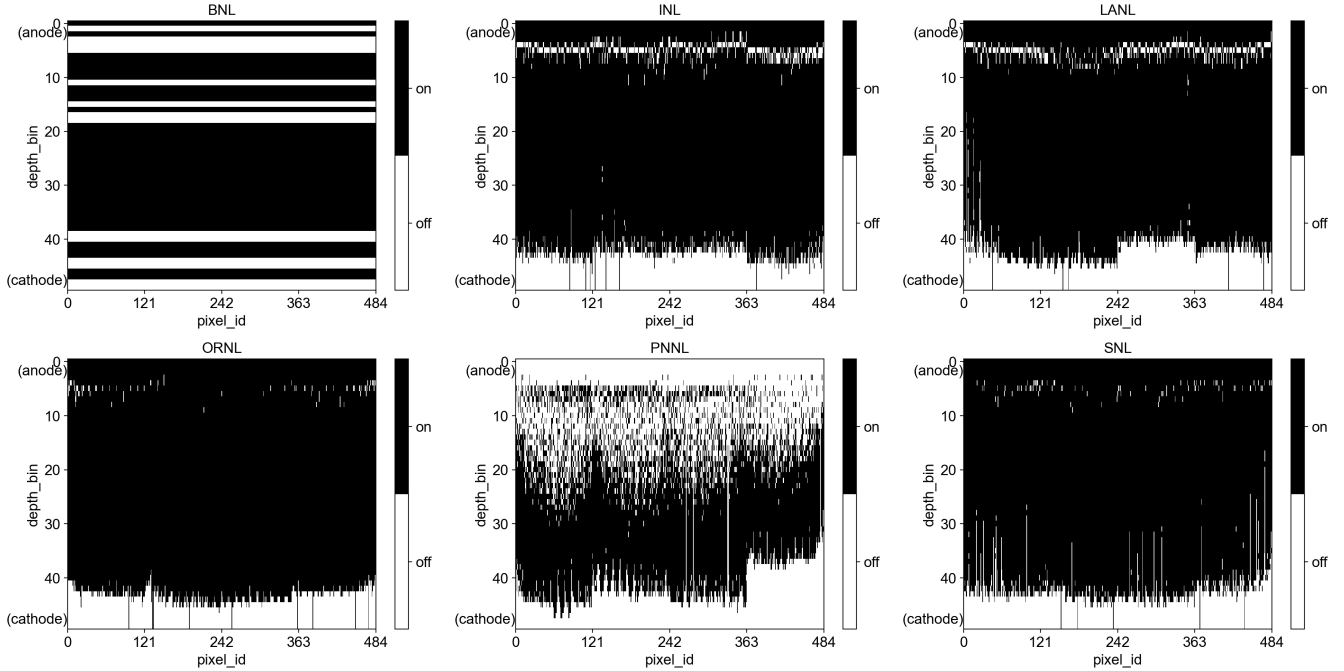


Fig. 4. Best cluster mask from each detector optimization.

TABLE II
SUMMARY OF TIME EFFICIENCY IMPROVEMENTS

detector	crossover time t^* [s]	speedup factor f_{30}	f_5
BNL	23	8.9	3.0
INL	39	11.7	5.2
LANL	68	8.9	3.0
ORNL	30	11.7	3.9
PNNL	117	5.2	2.3
SNL	17	15.4	5.2
mean	49	10.3	3.8

V. CONCLUSIONS

We have integrated the pyGEM uranium enrichment analysis code with the spectre-ml spectroscopic optimization framework, and shown that the uranium enrichment relative uncertainty can be directly used as an optimization target. This spectre-ml + GEM workflow provides a 20% relative improvement (averaged over six H3D M400 detectors) in the U-235 enrichment relative uncertainty in 30-minute long measurements, and retains similar enrichment accuracy to the unoptimized pyGEM-only results. These reductions in enrichment relative uncertainty can lead to significant time savings

for in-field nuclear safeguards inspections, with the optimized results achieving the same overall relative uncertainty as the unoptimized 30-minute measurements around $10\times$ faster. Future work could integrate other safeguards NDA software such as FRAM with spectre-ml for improved Pu spectroscopy, and investigate whether a single common optimization result can be applied across multiple detectors to provide improved spectroscopy with minimal operational cost.

APPENDIX

The following pseudocode provides a basic outline of the application programming interface (API) that an end-user would interact with to integrate their own analysis code with the spectre-ml framework.

```
# spectre-ml framework: abstract classes
class RankingMetric(ABC):
    ...
class SpectrumAnalyzer(ABC):
    ...

# user code: concrete becquerel workflow
class BecquerelSpectrumAnalyzer(SpectrumAnalyzer):
    def analyze(self):
```

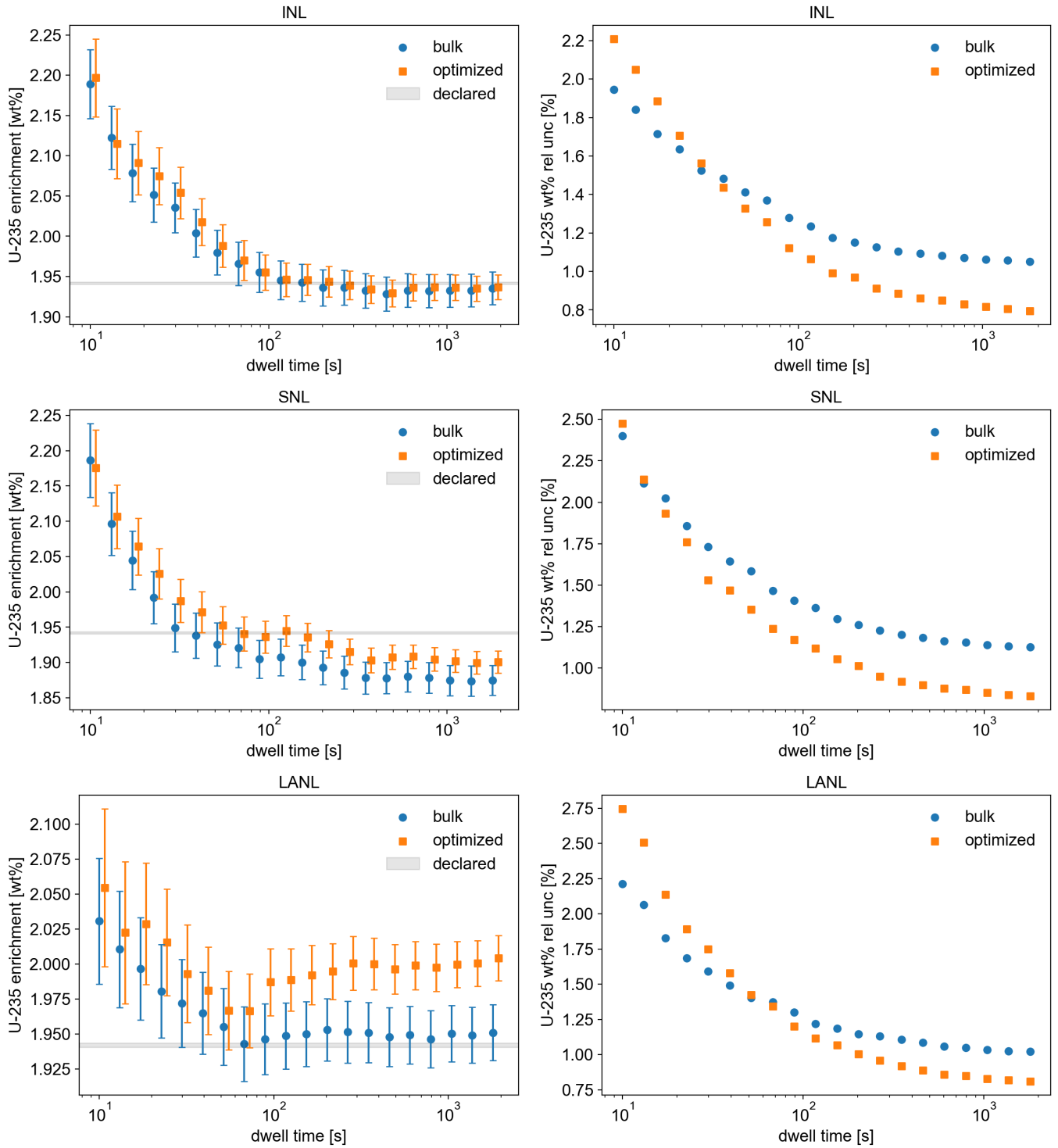


Fig. 5. Trends in pyGEM analysis metrics vs dwell time t , using the optimum long-dwell-computed mask from the INL (top row), SNL (middle row), and LANL (bottom row) detectors. Left column: U-235 enrichment (wt%). The optimized (orange) points are slightly offset along the x -axis from their corresponding bulk (blue) points for visual clarity. The gray band shows the SRM 969 certification of 1.9420 ± 0.0014 wt% [19]. Right column: U-235 relative uncertainty (%).

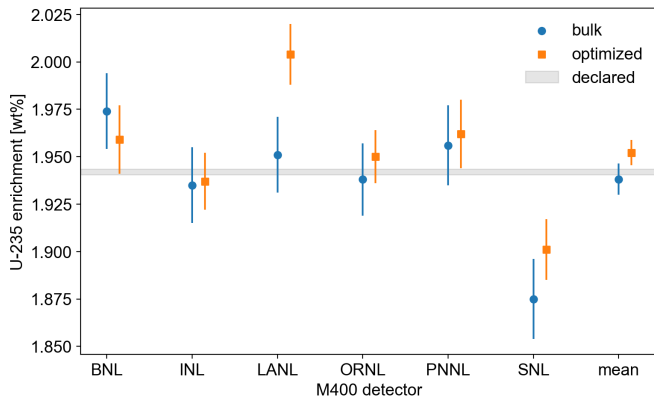


Fig. 6. Summary of U-235 enrichment assay results with (orange squares) and without (blue circles) the spectre-ml + pyGEM optimization.

```

compute_single_peak_fits()
class BecquerelRankingMetric(RankingMetric):
    def calc(self) -> float:
        return fit_param_rel_unc

# user code: two concrete pyGEM workflows
class GEMSpectrumAnalyzer(SpectrumAnalyzer):
    def analyze(self):
        compute_activity_calibration()
        compute_U235_region_fits()
class GEMEnrichmentMetric(RankingMetric):
    def calc(self) -> float:
        return enrichment_rel_unc
class GEMFittingMetric(RankingMetric):
    def calc(self) -> float:
        return fit_chi_squared

# user code: example GEM analysis
ms = spectre_ml.ModelSelector(
    spectrum_analyzer=GEMSpectrumAnalyzer(),
    ranking_metric=GEMEnrichmentMetric(),
    voxel_spectra=voxel_spectra,
    n_clusters=[2, 3],
    n_nmf_components=[2, 3],
    ...
)
ms.fit_models()
results = ms.evaluate_models()
results.plot()

```

ACKNOWLEDGMENTS

The authors thank Michael Streicher and David Goodman (H3D, Inc.) for useful discussions.

The U.S. Government retains, and the publisher, by accepting the article for publication, acknowledges, that the U.S. Government retains a non-exclusive, paid-up, irrevocable, world-wide license to publish or reproduce the published form of this manuscript, or allow others to do so, for U.S. Government purposes.

REFERENCES

[1] H3D, Inc., “M400 base specifications,” retrieved August 15, 2025 from <https://h3dgamma.com/M400Specs.pdf>.
[2] International Atomic Energy Agency, “Development and implementation support programme for nuclear verification 2022–2023,” International Atomic Energy Agency, Tech. Rep. STR-400, 2022.

[3] A. Lebrun, J. Beaumont, A. Berlizov, L. Bourva, Y. Dodane, D. Finker, M. Mayorov, and A. Sokolov, “The next generation of non-destructive assay tools for IAEA safeguards verification,” in *Symposium on International Safeguards: Reflecting on the Past and Anticipating the Future*, no. IAEA-CN-303, 2022, pp. 7–7.
[4] Y. Dodane, C. Schoch, S. Markin, and A. Lebrun, “Large-volume cadmium zinc telluride modules for safeguards verification of unirradiated nuclear material,” *Proc. INMM Annual Mtg*, 2023.
[5] D. I. Goodman, M. Streicher, C. June, B. Kitchen, C. G. Wahl, A. Driver, and W. Kaye, “Energy resolution and efficiency variations across commercial 3D pixelated CdZnTe crystals,” in *2022 IEEE Nuclear Science Symposium and Medical Imaging Conference (NSS/MIC)*. IEEE, 2022.
[6] J. R. Vavrek, H. S. Parrilla, G. Aversano, M. S. Bandstra, M. Folsom, and D. Hellfeld, “Data-driven performance optimization of gamma spectrometers with many channels,” *Accepted for publication at IEEE Transactions on Nuclear Science*. *arXiv preprint arXiv:2504.07166*, 2025.
[7] A. Bolotnikov, G. Camarda, G. Carini, Y. Cui, L. Li, and R. James, “Cumulative effects of Te precipitates in CdZnTe radiation detectors,” *Nuclear Instruments and Methods in Physics Research Section A: Accelerators, Spectrometers, Detectors and Associated Equipment*, vol. 571, no. 3, pp. 687–698, 2007.
[8] A. Berlizov, “GEM: A next-generation gamma enrichment measurements code,” *Journal of Nuclear Materials Management*, vol. 50, no. 1, pp. 110–120, 2022.
[9] Z. Li, J. Cheng, F. Liu, Q. Wang, W.-W. Wen, G. Huang, and Z. Wu, “Research on the technological progress of CZT array detectors,” *Sensors*, vol. 24, no. 3, p. 725, 2024.
[10] Y. Huang, Z. Tang, K. Zhang, B. Zhang, C. Gu, K. Liu, X. Liang, M. Cao, J. Wei, W. Liu *et al.*, “Machine learning optimization of CdZnTe crystal growth by the travelling heater method,” *Applied Crystallography*, vol. 58, no. 6, 2025.
[11] M. Petryk, K. Hinbern, W. Kaye, F. Zhang, S. Abraham, M. Streicher, A. Boucher, and Z. He, “Improved yield and performance of handheld radiation detectors using waveform-digitizing application-specific integrated circuits,” in *2025 IEEE Nuclear Science Symposium and Medical Imaging Conference (NSS/MIC)*. IEEE, 2025.
[12] S. Smith, R. Venkataraman, and S. Loftin, “Summary of the workshop on M400 high-resolution CZT detector safeguards applications,” Oak Ridge National Laboratory (ORNL), Oak Ridge, TN (United States), Tech. Rep. ORNL/SPR-2024/13, 2024, <https://doi.org/10.2172/2479046>.
[13] U. N. Roy, G. S. Camarda, Y. Cui, R. Gul, G. Yang, J. Zazvorka, V. Dedic, J. Franc, and R. B. James, “Evaluation of CdZnTeSe as a high-quality gamma-ray spectroscopic material with better compositional homogeneity and reduced defects,” *Scientific reports*, vol. 9, no. 1, p. 7303, 2019.
[14] J. Vavrek, M. Folsom, D. Hellfeld, H. Parrilla, and G. Aversano, “Spectral peak enhancement by combining trusted response elements via machine learning (spectre-ml) v0.8.0,” Lawrence Berkeley National Laboratory (LBNL), Berkeley, CA (United States), Tech. Rep., 2023.
[15] D. D. Lee and H. S. Seung, “Learning the parts of objects by non-negative matrix factorization,” *Nature*, vol. 401, no. 6755, pp. 788–791, 1999.
[16] Y.-X. Wang and Y.-J. Zhang, “Nonnegative matrix factorization: A comprehensive review,” *IEEE Transactions on knowledge and data engineering*, vol. 25, no. 6, pp. 1336–1353, 2012.
[17] S. Doniach and M. Sunjic, “Many-electron singularity in x-ray photoemission and x-ray line spectra from metals,” *Journal of Physics C: Solid State Physics*, vol. 3, no. 2, p. 285, 1970.
[18] B. S. McDonald, M. A. Zalavadia, K. D. Bensema, N. Deshmukh, E. Becker, L. E. Smith *et al.*, “Gamma-ray enrichment analysis of field-trial data from an unattended cylinder verification station,” *Journal of Nuclear Materials Management*, vol. 50, no. 1, pp. 43–57, 2022.
[19] S. D. Rasberry, “Standard reference material 969: uranium isotopic standard reference material for gamma spectroscopy measurements,” National Bureau of Standards, Office of Standard Reference Materials, Tech. Rep., 1985, <https://www.nrc.gov/docs/ML0512/ML051220510.pdf>.
[20] International Atomic Energy Agency, “International target values for measurement uncertainties in safeguarding nuclear materials,” International Atomic Energy Agency (IAEA), Tech. Rep. STR-368, 2022.
[21] —, “Physical models and algorithms of the NaGEM code (ver.2.1.x),” International Atomic Energy Agency, Tech. Rep. STR-395, 2020.
[22] W. Li, Z. He, G. Knoll, D. Wehe, and C. Stahle, “Spatial variation of energy resolution in 3-D position sensitive CZT gamma-ray spectrometers,” *IEEE Transactions on Nuclear Science*, vol. 46, no. 3, pp. 187–192, 1999.

- [23] T. E. Sampson, G. W. Nelson, and T. A. Kelley, "FRAM: A versatile code for analyzing the isotopic composition of plutonium from gamma-ray pulse height spectra." Los Alamos National Laboratory (LANL), Los Alamos, NM (United States), Tech. Rep. LA-11720-MS, 1989.